Spectroscopic properties and simulation of the energy level schemes of Nd^{3+} and Pr^{3+} ions in rare earth tellurium oxides

1992 J. Phys.: Condens. Matter 4 2721

(http://iopscience.iop.org/0953-8984/4/10/032)

J. Phys.: Condens. Matter 4 (1992) 2721–2734. Printed in the UK

Spectroscopic properties and simulation of the energy level schemes of Nd^{3+} and Pr^{3+} ions in rare earth tellurium oxides

C Cascales†, E Antic-Fidancev, M Lemaitre-Blaise and P Porcher
Laboratoire des Eléments de Transition dans les Solides, UPR associée au CNRS 210, 1, place Aristide Briand, F-92195 Meudon-Bellevue, France

Received 14 October 1991

Abstract. Absorption and emission measurements at liquid-helium temperature, liquid-nitrogen temperature and room temperature have been performed on monoclinic $RE_2Te_4O_{11}$ ($RE \equiv Nd^{3+}$, Pr^{3+}), on rare-earth tellurium oxides and on Pr-doped $Gd_2Te_4O_{11}$ samples, respectively. The rare earth occupies a single crystallographic position with a low point symmetry C_1. The spectra were analysed according to the crystal-field theory. From the experimental data, nearly complete energy level schemes of the Pr^{3+} and Nd^{3+}, on the $4f^2$ and $4f^3$ configurations, were derived. Very good correlation was obtained between the experimental and simulated energy level schemes, for the approximate C_{2v} and/or C_s site symmetries. The crystal-field parameters vary smoothly with the atomic number of the rare earth, when compared with those determined previously for Eu^{3+} in the same matrix.

1. Introduction

Although the rare-earth tellurates have been known for many years, the structure of compounds with $RE_2Te_4O_{11}$ stoichiometry has been described only recently [1]. This new host offers a good opportunity for a systematic study of the spectroscopic properties of the trivalent lanthanide ions, for several reasons: first, the $RE_2Te_4O_{11}$ structure contains only one crystallographic rare-earth site (with very low C_1 point symmetry, however); second, the compounds are isomorphic through the rare-earth series; finally, oxides with a lone pair of electrons, such as Sn(II), Sb(III) or Te(IV), possess important properties as luminescence activators [2].

A preliminary study of the optical properties of the europium tellurate $Eu_2Te_4O_{11}$ [3] emphasized the high quality of the spectroscopic data: many electronic transitions from different emitting levels, showing that the emission from upper excited levels is not quenched and narrow lines owing to a good crystallinity. The simulation of the Eu^{3+} energy level scheme was carried out with a low RMS deviation in spite of the low point site symmetry. All these features encouraged us to conduct further data collection and the crystal-field analysis of the two most frequently analysed rare-earth ions, Pr^{3+} and Nd^{3+}. The low-temperature absorption and luminescence spectra of those ions were

† Permanent address: Instituto de Ciencia de Materiales, D, Consejo Superior de Investigaciónes Científicas, Serrano 113, E-28006 Madrid, Spain.

0953-8984/92/102721 + 14 $04.50

studied and the results presented here. They were used to simulate the energy level schemes within the crystal-field theory, considering the free ion as well as the crystal-field parameters (CFPs).

2. Structural background

The family of the rare-earth tellurium oxides $RE_2Te_4O_{11}$ has been synthesized and characterized by x-ray diffraction techniques (4, 5). A recent study has reported the structure of $Nd_2Te_4O_{11}$ [1]. The compound belongs to the monoclinic system with $C2/c$ (No 15) as the space group. The unit-cell parameters are $a = 12.635$ Å, $b = 5.204$ Å, $c = 16.277$ Å and $\beta = 106.02°$ ($Z = 4$). The neodymium atom occupies only one atomic position of a C_1 point symmetry. The rare-earth atom is coordinated to eight oxygen atoms located at the corners of a distorted square antiprism. The NdO_8 polyhedra are linked together so that they form a two-dimensional subnetwork, with the $(Nd_2O_{10})_\infty$ composition. Another subnetwork of $(Te_8O_{21})_\infty$ two-dimensional sheets is found in the structure.

For the energy level simulation, the descending symmetry procedure by considering C_s or even C_{2v} as approximate point symmetry can be applied without difficulty.

3. Experimental details

3.1. Preparation of samples

Polycrystalline powder samples were prepared according to the method described previously [1]. Three samples were synthesized with praseodymium: the pure $Pr_2Te_4O_{11}$ and $Gd_2Te_4O_{11}$ activated by 1 and 5 mol.% Pr^{3+}. In the case of the Nd^{3+} ions, only the pure $Nd_2Te_4O_{11}$ compound was prepared, because no fluorescence measurements were attempted. The materials were tested by the x-ray diffraction technique, which showed only one phase.

3.2. Optical measurements

The absorption spectra of the pure praseodymium and neodymium compounds were obtained on a 3.4 m Jarrell–Ash grating spectrograph using photographic detection and on a Cary 2400 spectrometer. The measurements were carried out at 300, 77 and 4.2 K between 4000 and 30 000 cm^{-1}. The upper limit corresponds to the absorption edge of the matrix.

The fluorescence emission of the Pr^{3+}-doped samples were recorded at 300 and 77 K under various excitations: a 200 W UV mercury lamp equipped with a wide-band UV filter, the blue lines of a CW argon ion laser and/or a dye laser excitation accorded on selected crystal-field levels. The details of the experimental conditions can be found in [6] and [7].

4. Simulation of the energy level schemes

The spectroscopic properties of the rare-earth ions in crystalline matrices have received much attention since the early 1960s. This is due to the potential use of the rare-

earth compounds as laser materials and their interest in the modern technology as luminescence enhancers. They offer also an almost unique opportunity to compare the theory of the atomic spectra with high-precision experimental data, even when interactions of secondary importance are taken into account. The central-field approximation considers separately the Hamiltonians corresponding to the free-ion and crystal-field interactions, although the final purpose is to input them simultaneously in the secular determinant before diagonalization. According to the nomenclature of a rather recent review [8], the Hamiltonian used in the present study can be written as

$$\mathcal{H} = \mathcal{H}_0 - \sum_{k=0}^{k=3} E^k(nf, nf)e_k + \zeta_{4f}A_{SO} + \alpha L(L+1) + \beta G(G2) + \gamma G(R7) + \sum_{\substack{\lambda=2 \\ \lambda\neq 5}}^{\lambda=8} T^\lambda t_\lambda$$

where E^k and ζ_{4f} are the Racah parameters and the spin–orbit coupling constant, and e_k and A_{SO} represent the angular parts of the electrostatic repulsion and spin–orbit coupling, respectively. For the configurations of two or more equivalent electrons the two-body interactions are considered with the Tree parameters α, β and γ associated with Casimir operators $G(G_2)$ and $G(R_7)$. For configurations having more than two electrons, non-negligible three-body interactions can also be introduced (T^λ parameters). We do not consider here the spin–spin, spin–other-orbit and other relativistic interactions of minor importance which could be simulated through the $P^k(k = 2, 4, 6)$ and M_k $(k = 0, 2, 4)$ integrals.

In the present case, seven free-ion parameters can describe adequately the $4f^2$ configuration of Pr^{3+}. Since the $^1S_0$ level is only observed by the means of two-photon spectroscopy [9], the γ-parameter was fixed to a standard value (table 1). For the $4f^3$ configuration of Nd^{3+} the T^λ parameters are introduced, too. For the same reasons as for Pr^{3+}, some parameters (γ, T^2 and T^8) were fixed to values used in earlier studies [9–11].

The crystal-field calculations are usually carried out within the single-particle crystal-field theory [12, 13]. Following Wybourne's formalism the crystal-field Hamiltonian is expressed as a sum of products of spherical harmonics and CFPs:

$$H_{cf} = \sum \{B_q^k[C_q^k + (-1)^q C_q^k] + iS_q^k[C_q^k - (-1)^q C_q^k]\}.$$

The number of the non-zero S_q^k and B_q^k CFPs depends on the crystallographic point site symmetry of the lanthanide ion. For the C_1 site symmetry there are 27 parameters which are non-realistic conditions for a simulation. Therefore, we consider the approximate C_s symmetry close to the true symmetry. However, in order to make the simulation carefully, we carry out the descending symmetry procedure in several steps.

(i) The first simulation is performed for the approximate C_{2v} symmetry; all S_q^k parameters of the crystal-field Hamiltonian vanish, which gives a total of nine CFPs.

(ii) The nine CFPs thus obtained are considered as starting parameters for the simulation for the C_s symmetry, which now gives six additional non-zero S_q^k parameters. The 15 CFPs are, however, reduced to 14 by a proper choice of the reference axis system, cancelling S_2^2. This set is, in the present case, the most reasonable approach to the true symmetry.

The procedure to obtain the CFPs could be hardly facilitated if the CFP starting values had been estimated by a calculation from atomic positions. The most simplified model considers the effect of the electrostatic point charges (PCEM) localized at the crystallographic sites of the atoms on the network. Recent attempts have also included

Table 1. Free-ion and crystal-field parameters for $RE_2Te_4O_{11}$ (RE = Pr, Nd, Eu). The values in square brackets indicate parameters not varied. The values in parentheses are the estimated standard deviations. Units in cm^{-1}.

	Pr		Nd		Eu[a]	
	C_{2v}	C_s	C_{2v}	C_s	C_{2v}	C_s
E_0	5369(2)	5381(2)	12958(1)	12964(1)		
E_1	4417(2)	4413(2)	4932.4(8)	4932.7(7)		
E_2	22.09(2)	22.16(2)	23.37(2)	23.34(1)		
E_3	459.4(2)	459.6(1)	480.94(9)	480.94(9)		
α	21.74(7)	22.16(6)	20.32(4)	20.41(4)		
β	−591(2)	−613(2)	−611(1)	−619(1)		
γ	[1540]	[1540]	[750]	[750]		
ζ	746.2(9)	746.4(8)	873.0(7)	873.5(6)		
T^2			[294.4]	[294.4]		
T^3			32(2)	32(2)		
T^4			91(3)	91(2)		
T^6			−248(6)	−248(6)		
T^7			305(7)	302(6)		
T^8			[222]	[222]		
B_0^2	283(14)	212(13)	416(19)	354(20)	235(23)	226(23)
B_2^2	−107(12)	−57(10)	−191(12)	−202(14)	−187(16)	−168(17)
B_0^4	1717(28)	1733(23)	1165(34)	1068(34)	1327(51)	1346(47)
B_2^4	756(20)	889(18)	744(27)	650(31)	563(34)	451(37)
S_2^4	—	165(45)	—	656(31)	—	423(40)
B_4^4	367(25)	74(40)	401(30)	367(37)	632(39)	430(40)
S_4^4	—	−241(26)	—	6(44)	—	402(62)
B_0^6	831(43)	616(41)	−144(45)	25(54)	−484(59)	−265(60)
B_2^6	83(38)	99(36)	238(38)	165(46)	536(42)	472(47)
S_2^6	—	45(47)	—	−124(46)	—	−23(40)
B_4^6	−734(29)	−172(40)	−522(31)	−454(32)	−615(40)	−648(53)
S_4^6	—	710(29)	—	341(40)	—	100(44)
B_6^6	−482(40)	−273(41)	−332(30)	−232(35)	−485(38)	−379(36)
S_6^6	—	561(37)	—	136(65)	—	153(103)
Levels	52	52	103	103	23	23
σ	22.4	15.4	25.8 21.8[b]	22.7 17.8[b]	12.1	9.7
Residue	18086	7318	55240 39516[b]	40130 24578[b]	2041	844

[a] See [3].
[b] Values obtained with $U^4/_4$ reduced tables (see text).

dipolar and quadrupolar contributions [14–19]. A more pragmatic approach was successfully applied for various compounds of scheelite-type structure [20]. Accordingly we carried out calculations by using this 'three-parameter method', considering an effective charge for oxygen and tellurium ions [20, 21]. Unfortunately, these CFPs are too far from the experimental result. This is probably a consequence of the existence of covalent tellurium oxygen complex groups for which the ionic effective charge has no real significance. Finally, the best method is to consider the CFPs as phenomenological parameters to be derived from spectroscopic data.

The phenomenological CFPs of the trivalent europium are a convenient set of starting values for crystal-field calculations [3, 6]. Since the ground ^7F septet of the $4f^6$ con-

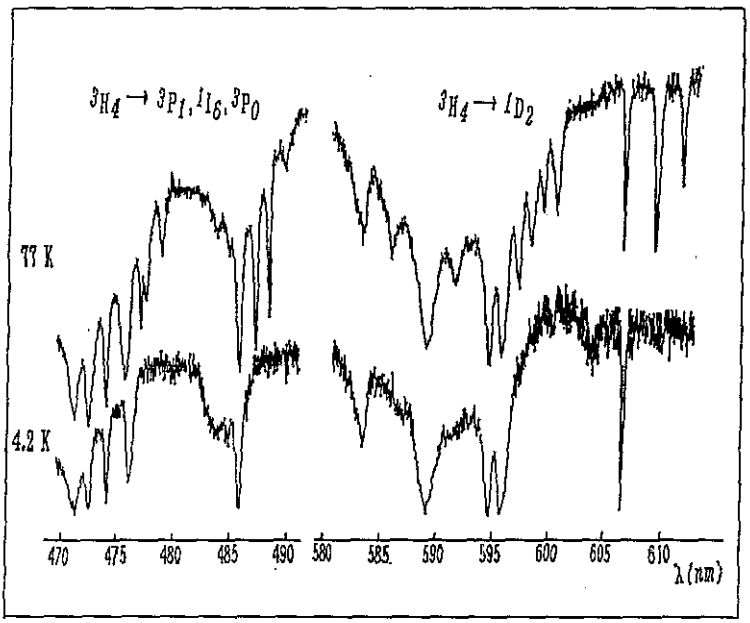

Figure 1. Comparison of part of the absorption spectra of $Pr_2Te_4O_{11}$ at 77 and 4.2 K.

figuration is well isolated from the rest of the configuration and is the only one of that multiplicity, an accurate simulation of the crystal-field effect is allowed by considering only the strongly reduced $^7F_{JM}$ basis, i.e. 49 $|SLJM_J\rangle$ states. In addition CFPs should vary smoothly in an isostructural series. All simulations are performed by the FORTRAN computer programs REEL and IMAGE [22].

5. Results and discussion

5.1. $Pr_2Te_4O_{11}$ and $Gd_2Te_4O_{11}$:Pr

All observed transitions in the absorption spectrum of $Pr_2Te_4O_{11}$ are sharp and well resolved (figure 1). The J-manifolds of $Pr_2Te_4O_{11}$ are split in the maximum number of $J + \frac{1}{2}$ Stark components (table 2). Absorption spectra at 4.2 K of pure $Pr_2Te_4O_{11}$ show only one line corresponding to the $^3H_4 \rightarrow {}^3P_0$ transition; at liquid-helium temperature, only the lowest Stark level of the ground level is thermally populated. The existence of only one crystallographic point site occupied by the rare earth is thus confirmed. The lack of selection rules for electric and magnetic dipole transitions for the C_1 symmetry allows one to draw an almost full sequence for $^1D_2$, $^3P_{0,1,2}$ levels and some Stark components of the $^1I_6$ singlet.

The luminescence spectra show that at 77 K the $^3P_0$ is the main emitting level, and almost all possible transitions between Stark levels can be observed (figure 2). The fluorescence emission from $^1D_2$ has a lower intensity and not all transitions allowed are observed.

A scheme of 52 energy levels was considered in both simulations with the C_{2v} and C_s point symmetries. The simulations yielded energy level schemes in good agreement with

Table 2. Observed and calculated energy levels for $Pr_2Te_4O_{11}$ and $Gd_2Te_4O_{11}$: Pr.

State $^{2S+1}L_J$	Energy level (cm^{-1})				
		Calculated			
	Experimental	C_{2v}	$C_{2v(experimental-calculated)}$	C_s	$C_{s(experimental-calculated)}$
$^3H_4$	0	−9	9	0	9
	90	117	−27	91	−1
	147	165	−18	143	4
	250	213	37	234	16
	352	341	11	358	−6
	437	464	−27	445	−8
	—	497	—	486	—
	528	510	18	535	−7
	620	637	−17	622	−2
$^3H_5$	2 212	2 206	6	2 215	−3
	2 224	2 229	−5	2 229	−5
	2 261	2 280	−19	2 273	−12
	2 278	2 296	−18	2 290	−12
	2 421	2 400	21	2 414	7
	2 439	2 442	−2	2 433	6
	2 493	2 487	6	2 484	9
	2 541	2 505	36	2 521	20
	—	2 600	—	2 599	—
	2 645	2 636	9	2 631	14
	2 685	2 677	8	2 678	7
$^3H_6$	4 307	4 314	−7	4 303	4
	4 320	4 326	−6	4 335	−15
	4 362	4 364	−2	4 365	−3
	4 385	4 373	12	4 377	8
	—	4 444	—	4 476	—
	4 540	4 550	−10	4 545	−5
	4 587	4 631	−44	4 600	−13
	4 679	4 659	20	4 663	16
	—	4 729	—	4 702	—
	—	4 800	—	4 822	—
	—	4 858	—	4 844	—
	4 923	4 904	19	4 930	−7
	—	4 941	—	4 937	—
$^3F_2$	5 082	5 071	11	5 090	−8
	5 150	5 133	17	5 155	−5
	5 161	5 180	−19	5 186	−25
	5 185	5 224	−39	5 199	−14
	5 242	5 230	12	5 220	22
$^3F_3$	6 448	6 436	12	6 440	8
	6 486	6 457	29	6 476	10
	6 507	6 491	16	6 492	15
	6 526	6 552	−26	6 534	−8
	6 549	6 561	−12	6 547	2
	—	6 571	—	6 577	—
	—	6 656	—	6 657	—

Table 2 *continued*

State $^{2S+1}L_J$	Energy level (cm^{-1})				
		Calculated			
	Experimental	C_{2v}	$C_{2v(experimental-calculated)}$	C_s	$C_{s(experimental-calculated)}$
$^3F_4$	—	6 815		6 776	—
	6 850	6 852	−2	6 818	−2
	—	6 870	—	6 827	—
	6 896	6 875	21	6 870	26
	6 931	6 916	15	6 937	−6
	7 006	7 001	5	7 016	−10
	7 060	7 094	−34	7 091	−31
	7 096	7 096	0	7 097	−1
	7 124	7 135	−11	7 125	−1
$^1D_2$	16 477	16 479	−2	16 483	−6
	16 778	16 775	3	16 779	−1
	16 840	16 856	−16	16 837	3
	16 958	16 965	−7	16 966	−8
	17 120	17 098	22	17 107	13
$^3P_0$	20 525	20 509	16	20 515	10
$^1I_6$	20 965	20 980	−15	20 979	−14
$^3P_1$	21 049	21 035	14	21 035	14
	21 141	21 143	−2	21 147	−6
	21 200	21 214	−14	21 204	−4

the experimental data (table 2). The simulation was undoubtedly improved when the S_q^k-parameters were introduced since the RMS standard deviation as well as the residue decreased significantly (table 1).

5.2. $Nd_2Te_4O_{11}$

Transitions in the absorption spectrum of Nd^{3+} at liquid-helium temperature originate from the lowest Stark component of the $^4I_{9/2}$ ground-state manifold. Figure 3 shows an example of this very well resolved spectrum, where lines are unambiguously attributed. The energy positions of the $^4I_{9/2}$ crystal-field components have been established from the transition to $^2P_{1/2}$ at 300 K. One could establish rapidly a quite complete energy level scheme of 103 of a total of 182 from absorption measurements. Table 3 gives the experimental Stark components of $Nd_2Te_4O_{11}$ up to 30 000 cm^{-1}. The relatively large number of levels offers a good opportunity for a free-ion and crystal-field calculation in spite of the low point symmetry. As for Pr^{3+}, the simulations were performed for the C_{2v} and the C_s symmetries. Despite the number of parameters the C_s simulation yields a better reproduction of the experimental energy level scheme, with a lower RMS standard deviation and without large individual discrepancies between experimental and calculated values for most levels. However, an exception is observed in the simulation of the $^2H_{11/2}$ level splitting. This situation is very common for the Nd^{3+} configuration [23].

Table 3. Observed and calculated energy levels for $Nd_2Te_4O_{11}$.

Level $^{2S+1}L_J$	Energy level (cm^{-1})				
		Calculated			
	Experimental	C_{2v}	$C_{2v(experimental-calculated)}$	C_s	$C_{s(experimental-calculated)}$
$^4I_{9/2}$	0	5	−5	−2	2
	95	117	−22	111	−16
	192	202	−10	203	−11
	254	252	2	253	1
	347	383	−36	379	−32
$^4I_{13/2}$	3 905	3 892	13	3 892	13
	3 943	3 911	32	3 921	22
	4 001	4 004	−3	3 997	4
	4 042	4 050	−8	4 030	12
	4 089	4 086	3	4 087	2
	4 136	4 119	17	4 122	14
	4 161	4 138	23	4 149	12
$^4I_{15/2}$	5 855	5 857	−2	5 851	4
	5 900	5 879	21	5 892	8
	5 995	5 993	2	5 993	2
	6 059	6 084	−25	6 068	−9
	6 158	6 166	−8	6 161	−3
	6 228	6 197	31	6 212	16
	6 240	6 250	−10	6 235	5
	6 294	6 283	11	6 304	−10
$^4F_{3/2}$	11 381	11 364	17	11 366	15
	11 470	11 443	27	11 440	30
$^4F_{5/2}$	12 392	12 375	17	12 378	14
	12 475	12 441	34	12 434	41
	12 507	12 490	17	12 503	4

$^2H_{9/2}$	12 564	12 578		−14		12 577		−13	
	12 614	12 603		11		12 602		12	
	12 637	12 634		3		12 636		1	
	12 688	12 713		−25		12 709		−21	
$^4F_{7/2}$	13 346	13 365		−19		13 369		−23	
	13 406	13 410		−4		13 415		−9	
	13 447	13 449		−2		13 450		−3	
$^4S_{3/2}$	13 453	13 466		−13		13 468		−15	
	13 490	13 475		15		13 478		12	
$^4F_{7/2}$	13 506	13 525		−19		13 524		−18	
$^4F_{9/2}$	14 608	14 630		−22		14 629		−21	
	14 639	14 657		−18		14 661		−22	
	14 686	14 691		−5		14 691		−5	
	14 763	14 786		−23		14 792		−29	
	14 822	14 803		19		14 807		15	
$^2H_{11/2}$	15 814	15 887	15 841[a]	−73	−27[a]	15 888	15 836[a]	−74	−22[a]
	15 838	15 903	15 864[a]	−65	−26[a]	15 905	15 862[a]	−67	−24[a]
	15 891	15 916	15 888[a]	−25	−25[a]	15 911	15 886[a]	−20	5[a]
	15 933	15 922	15 927[a]	11	6[a]	15 925	15 933[a]	8	0[a]
	15 986	15 928	15 981[a]	58	5[a]	15 931	15 988[a]	55	−2[a]
	16 004	15 949	16 003[a]	55	1[a]	15 949	16 007[a]	55	−3[a]
$^4G_{5/2}$	16 905	16 935		−30		16 927		−22	
	17 034	17 032		2		17 031		3	
	17 139	17 112		27		17 116		23	
$^4G_{7/2}$	17 173	17 213		−40		17 196		−23	
	17 223	17 235		−12		17 229		−6	
$^2G_{7/2}$	17 281	17 283		−2		17 260		21	
$^4G_{5/2}$	17 374	17 310		64		17 348		26	
$^4G_{7/2}$	18 858	18 839		19		18 846		12	
	18 908	18 913		−5		18 883		25	
	18 946	18 945		1		18 954		−8	
	19 016	19 003		13		18 992		24	

Table 3 *continued*

Level $^{2S+1}L_J$	Energy level (cm^{-1})				
		Calculated			
	Experimental	C_{2v}	$C_{2v(experimental-calculated)}$	C_s	$C_{s(experimental-calculated)}$
$^2K_{13/2}$	19 249	19 217	32	19 232	17
	19 319	19 334	−15	19 319	0
$^4G_{9/2}$	19 381	19 387	−6	19 389	−8
	19 409	19 398	11	19 409	0
	19 434	19 434	0	19 430	4
	19 449	19 448	1	19 456	−7
	19 461	19 452	9	19 475	−14
$^2K_{13/2}$	19 555	19 553	2	19 543	12
	19 623	19 602	21	19 610	13
	19 658	19 657	1	19 660	−2
	19 706	19 727	−21	19 713	−7
	19 778	19 768	10	19 771	7
$^2G_{9/2}$	20 878	20 856	22	20 855	23
	20 907	20 866	41	20 883	24
	20 923	20 916	7	20 918	5
	20 959	20 969	−10	20 955	4
	20 977	20 014	−37	20 986	−9
$^2D_{3/2}$	21 083	21 086	−3	21 089	−6
	21 130	21 113	17	21 120	10
$^4G_{11/2}$	21 194	21 233	−39	21 219	−25
	21 233	21 264	−31	21 269	−36
$^2K_{15/2}$	21 332	21 335	−3	21 325	7
	21 395	21 360	35	21 376	19
$^4G_{11/2}$	21 411	21 415	−4	21 402	9
	21 460	21 482	−22	21 499	−39

$^2K_{15/2}$	21 526	21 522	4	21 537	−11
	21 609	21 605	4	21 616	−7
$^4G_{11/2}$	21 639	21 631	8	21 633	6
	21 652	21 662	−10	21 665	−13
	21 687	21 678	9	21 678	9
$^2K_{15/2}$	21 735	21 732	3	21 716	19
	21 783	21 743	40	21 765	18
$^2P_{1/2}$	23 147	23 134	13	23 133	14
$^2D_{5/2}$	23 640	23 628	12	23 631	9
	23 721	23 721	0	23 727	−6
	23 791	23 807	−16	23 798	−7
$^2P_{3/2}$	26 032	26 019	13	26 019	13
	26 103	26 110	−7	26 105	−2
$^4D_{3/2}$	27 784	27 790	−6	27 795	−11
	27 840	27 853	−13	27 832	8
$^4D_{5/2}$	—	27 926		27 881	—
	28 050	27 987	63	28 027	23
	28 243	28 238	5	28 232	11
$^4D_{1/2}$	28 421	28 444	−23	28 437	−16
$^2I_{11/2}$	29 125	29 142	−17	29 132	−7
	29 244	29 265	−21	29 245	−1
	29 320	29 319	1	29 333	−13

[a] Energy level values obtained with $U^4/4$ reduced tables (see text).

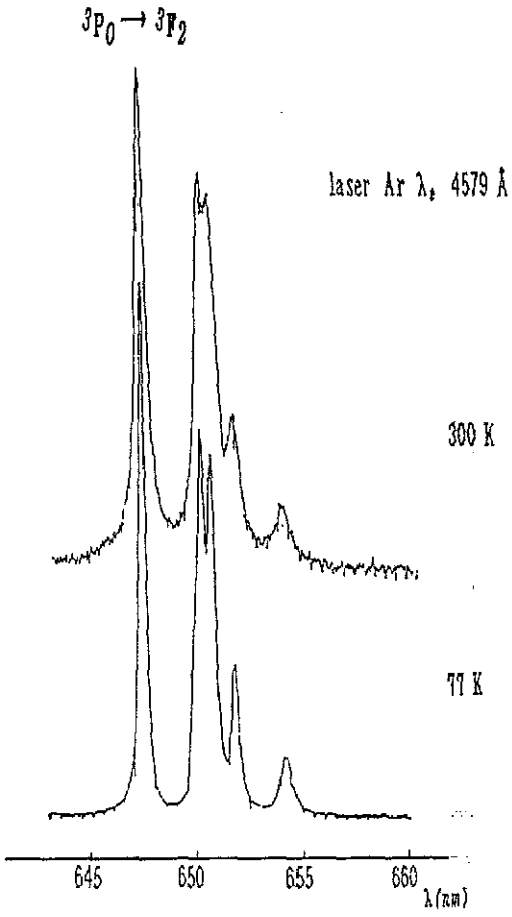

Figure 2. Part of the fluorescence spectrum for $Gd_2Te_4O_{11}$: Pr^{3+} at 4.2 K and λ_e = 457.9 nm (argon laser).

It has been recently argued [24] that a non-negligible mixing of that level with some states of the $4f^2$ 5d excited configuration occurs through the *odd* terms in the expansion of the crystal-field Hamiltonian, also taken into account in the phenomenological simulation of the electric dipole transition intensities [25]. This assumption is difficult to handle because of the larger secular determinant. A more empirical method to ameliorate the simulation is to divide the $\langle {}^2H(1)_{11/2}|U^4|{}^2H(1)_{11/2}\rangle$ reduced matrix element by 4 [23]. This process improves the simulation, almost without changing the CFPs values, and reduces the residue ($\Sigma|E_{exp} - E_{calc}|^2$) as well as the RMS standard deviation. The results are given in tables 1 and 3.

Table 1 also compares the phenomenological CFPs for Pr^{3+}, Nd^{3+} and Eu^{3+}. Some of the Eu^{3+} CFPs are slightly different from those reported previously [3]. The set of new values reported here for this ion is obtained from a new attempt at simulation using starting values extrapolated from Pr^{3+} and Nd^{3+}. This is really a self-consistent method because the older set of Eu^{3+} CFPs has been considered as starting values for Pr^{3+} and Nd^{3+}. Anyway, the difference between [3] and here emphasizes the great difficulty in simulating an energy level scheme when the number of CFPs is large, i.e. when the point symmetry is low and when there are neither starting values calculated from *a priori* models for these parameters, nor experimental values obtained under polarized light.

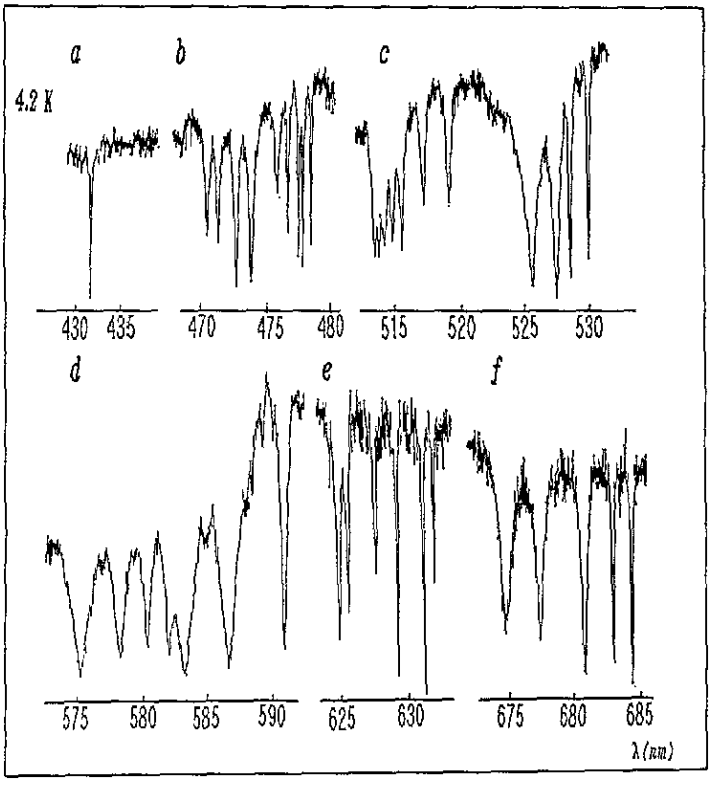

Figure 3. Part of the absorption spectrum of $Nd_2Te_4O_{11}$ at 4.2 K for various transitions: (*a*) $^4I_{9/2} \rightarrow {}^2P_{1/2}$; (*b*) $^4I_{9/2} \rightarrow {}^4G_{11/2}$, $^2G_{9/2}$; (*c*) $^4I_{9/2} \rightarrow {}^4G_{9/2}$, $^2K_{13/2}$, $^4G_{7/2}$; (*d*) $^4I_{9/2} \rightarrow {}^2G_{7/2}$, $^4G_{5/2}$; (*e*) $^4I_{9/2} \rightarrow {}^2H_{11/2}$; (*f*) $^4I_{9/2} \rightarrow {}^4F_{9/2}$.

It seems that the only and relatively secure way for operating such a simulation is to perform simultaneous simulations on various electronic configurations. $4f^2$, $4f^3$ and $4f^6$ configurations of trivalent Pr, Nd and Eu ions are the most appropriate cases. The simulation will be considered as good when the sets of CFPs only vary smoothly along an isostructural matrix series.

Acknowledgments

We express our gratitude to Dr A Castro for providing the samples, and to Dr J Hölsä for various helpful discussions. One of the authors (CC) acknowledges the fellowship from the Consejo Superior de Investigaciónes Científicas, Spain.

References

[1] Castro A, Enjalbert R, Lloyd D, Rasines I and Galy J 1990 *J. Solid State Chem.* **85** 100
[2] Blasse G 1983 *Rev. Inorg. Chem.* **5** 328

[3] Cascales C, Antic-Fidancev E, Lemaitre-Blaise M and Porcher P 1991 *J. Alloys and Compounds* at press
[4] Redman M J, Binnie W P and Carter J R 1968 *J. Less-Common Met.* **16** 407
[5] Parada C, Alonso J A and Rasines I 1986 *Inorg. Chim. Acta* **111** 197
[6] Cascales C, Antic-Fidancev E, Lemaitre-Blaise M and Porcher P 1990 *J. Solid State Chem.* **89** 118
[7] Antic-Fidancev E, Lemaitre-Blaise M, Krupa J C and Porcher P 1991 *Eur. J. Solid State Inorg. Chem.* **28** 81
[8] Carnall W T, Goodman G L, Rajnak K and Rana R S 1989 *J. Chem. Phys.* **90** 3443
[9] Antic-Fidancev E, Lemaitre-Blaise M, Beaury L, Teste de Sagey G and Caro P 1980 *J. Chem. Phys.* **73** 4613
[10] Caro P, Svoronos D R, Antic-Fidancev E and Quarton M 1977 *J. Chem. Phys.* **66** 5284
[11] DaGama A A S, De Sa G F, Porcher P and Caro P 1981 *J. Chem. Phys.* **75** 2583
[12] Wybourne B G 1965 *Spectroscopic Properties of Rare Earths* (New York: Wiley)
[13] Hüfner S 1978 *Optical Spectra of Transparent Rare Earth Compounds* (New York: Academic)
[14] Faucher M and Garcia D 1982 *Phys. Rev.* B **262** 5451
[15] Morrison C A, Leavitt R P and Wortman D E 1980 *J. Chem. Phys.* **763** 2580
[16] Faulkner T R and Richarson F S 1980 *Mol. Phys.* **39** 75
[17] Faucher M, Dexpert-Ghys J and Caro P 1980 *Phys. Rev.* B **21** 3689
[18] Morrison C A 1976 *Solid State Commun.* **18** 153
[19] Newman D J 1971 *Adv. Phys.* **20** 197
[20] Leavitt R P, Morrison C A and Wortman D E 1975 *Harry Diamond Laboratories (Adelphi, MA) Report* HDL-TR-1673
[21] Huang J 1983 *PhD Thesis* Université Pierre et Marie Curie, Paris
[22] Porcher P 1989 *Computer programs* REEL *and* IMAGE *for simulation of d^n and f^n configurations involving real and complex crystal field parameters* unpublished
[23] Faucher M, Garcia D and Porcher P 1989 *Ct. R. Acad. Sci., Paris* **308** Ser. II 603
[24] Garcia D and Faucher M 1989 *J. Chem. Phys.* **90** 5280
[25] Judd B R 1962 *Phys. Rev.* **127** 750